

# On the formation of niacin (vitamin B3) and pyridine carboxylic acids in interstellar model ices



Brandon M. McMurtry<sup>a,b</sup>, Andrew M. Turner<sup>a,b</sup>, Sean E.J. Saito<sup>a,b</sup>, Ralf I. Kaiser<sup>a,b,\*</sup>

<sup>a</sup> W. M. Keck Research Laboratory in Astrochemistry, University of Hawaii at Manoa, Honolulu, Hawaii, HI 96822, United States

<sup>b</sup> Department of Chemistry, University of Hawaii at Manoa, Honolulu, Hawaii, HI 96822, United States

## ARTICLE INFO

### Article history:

Received 28 October 2015

In final form 14 March 2016

Available online 26 March 2016

### Keywords:

Astrochemistry

Astrobiology

Meteorites

Solid state

Origins of Life

## ABSTRACT

The formation of pyridine carboxylic acids in interstellar ice grains was simulated by electron exposures of binary pyridine (C<sub>5</sub>H<sub>5</sub>N)-carbon dioxide (CO<sub>2</sub>) ice mixtures at 10 K under contamination-free ultrahigh vacuum conditions. Chemical processing of the pristine ice and subsequent warm-up phase was monitored on line and in situ via Fourier transform infrared spectroscopy to probe for the formation of new radiation induced species. In the infrared spectra of the irradiated ice, bands assigned to nicotinic acid (niacin; vitamin B3; *m*-C<sub>5</sub>H<sub>4</sub>NCOOH) along with 2,3-, 2,5-, 3,4-, and 3,5-pyridine dicarboxylic acid (C<sub>5</sub>H<sub>3</sub>N(COOH)<sub>2</sub>) were unambiguously identified along with the hydroxycarbonyl (HOCO) radical. Our study suggests that the reactive pathway responsible for pyridine carboxylic acids formation involves a HOCO intermediate, which forms through the reaction of suprathreshold hydrogen ejected from pyridine with carbon dioxide. The newly formed pyridinyl radical may then undergo radical–radical recombination with a hydroxycarbonyl radical to form a pyridine carboxylic acid.

© 2016 Elsevier B.V. All rights reserved.

## 1. Introduction

Nicotinic acid (*m*-C<sub>5</sub>H<sub>4</sub>NCOOH) – commonly known as vitamin B3 or niacin – along with the other two monosubstituted pyridine carboxylic acids, picolinic acid (*o*-C<sub>5</sub>H<sub>4</sub>NCOOH) and isonicotinic acid (*p*-C<sub>5</sub>H<sub>4</sub>NCOOH; Fig. 1), have recently been identified in the carbonaceous chondrites Murchison [1,2] and Tagish Lake [3] at levels of typically 7 ppm. A follow-up study by Smith et al. [4] on CM2-type carbonaceous chondrites revealed the presence of three monosubstituted pyridine carboxylic acid isomers at levels from 163 to 1377 ppb along with three disubstituted pyridine carboxylic acids (2,5-, 3,4-, and 3,5-) (Fig. 1). These findings build upon the complex inventory of organic molecules detected within chondrites [5] including (polycyclic) aromatic hydrocarbons [6,7], nucleobases [8], sugars [9,10], and amino acids [11–13]. Detailed <sup>13</sup>C/<sup>12</sup>C, <sup>15</sup>N/<sup>14</sup>N, and D/H isotopic analysis explicitly indicated an interstellar origin of these biorelevant molecules [1,2,7]. Among these complex organic molecules, nicotinic acid (*m*-C<sub>5</sub>H<sub>4</sub>NCOOH) in particular has received considerable attention due to its crucial role in biological systems by serving as an important precursor to the redox coenzymes nicotinamide adenine dinucleotide (NAD) and nicotinamide adenine dinucleotide phosphate (NADP) – key components to cellular metabolic reactions [4]. Within the scope

of modern metabolisms, NAD and NADP, in coordination with enzymes, promote the replication and repair of deoxyribonucleic acid (DNA), the ligation of ribonucleic acid (RNA), and cell differentiation through transfer of its nucleotidyl moiety to nucleic acids and proteins [14]. NAD has also been proposed as a potential catalyst to protometabolism on prebiotic Earth and to the origin of RNA [15,16]. These diverse implications of NAD in the prebiotic formation of complex, biorelevant molecules emphasize the importance of nicotinic acid in early Earth environments.

Despite the importance of nicotinic acid (*m*-C<sub>5</sub>H<sub>4</sub>NCOOH) in astrobiology and its role in the *Origins of Life* theme, little is known on the underlying formation pathways in extraterrestrial environments [14]. Conducting a retrosynthesis [17], the nicotinic acid molecule can be formally decomposed into a pyridine molecule (C<sub>5</sub>H<sub>5</sub>N) plus carbon dioxide (CO<sub>2</sub>). Since both molecules represent closed shell molecules in their <sup>1</sup>A<sub>1</sub> and <sup>1</sup>Σ<sub>g</sub><sup>+</sup> electronic ground states, the reaction of pyridine with carbon dioxide to form nicotinic acid in the gas phase is afflicted with a significant entrance barrier [18,19], which cannot be overcome in cold molecular clouds holding averaged translational temperatures of typically 10 K. Further, even if formed in the gas phase via the reaction of pyridine with carbon dioxide at elevated temperatures, a third body collider is required to carry away the internal energy of the nicotinic acid prior to its unimolecular decomposition; however, due to the low number densities of typically 10<sup>−4</sup>–10<sup>−5</sup> cm<sup>−3</sup> in cold molecular clouds, only bimolecular reactions take place.

\* Corresponding author.

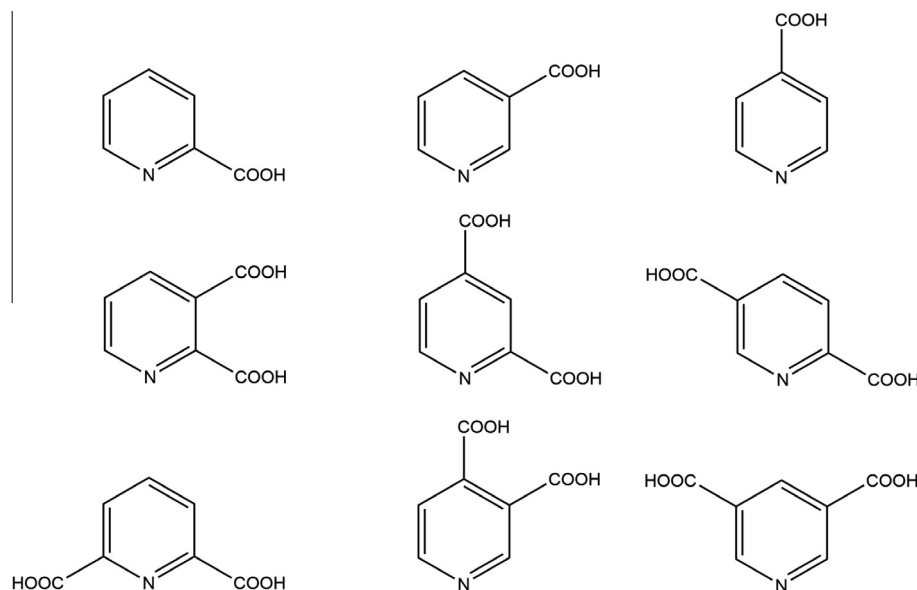
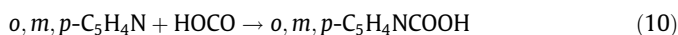


**Fig. 1.** Nine mono- and disubstituted pyridine carboxylic acid species. Of particular interest is nicotinic acid ( $m$ - $C_5H_4NCOOH$ ; top, center) due to its biological significance in terrestrial environments. In addition to the full suite of monosubstituted pyridine carboxylic acids (top), 2,5- (middle, right), 3,4- (bottom, center), and 3,5- (bottom, right) disubstituted pyridine carboxylic acids have recently been identified within a series of CM2-type carbonaceous chondrites.

As a consequence, formation of nicotinic acid in the gas phase of the interstellar medium is problematic. On the other hand, complex organic molecules and carboxylic acids (RCOOH) in particular have been shown to be formed in laboratory experiments in interstellar analog ices upon exposure to ionizing radiation such as ultraviolet photons, galactic cosmic rays, and energetic electrons simulating the secondary electrons generated via the interaction of galactic cosmic ray particles with interstellar ices [20,21]. More specifically, formic acid (HCOOH) [22], acetic acid (CH<sub>3</sub>COOH) [17], and complex organic carboxylic acids with 'R' being an organic alkyl group (RCOOH) [21] were formed in water–carbon monoxide, methane–carbon dioxide, and carbon dioxide–hydrocarbon ices, respectively, upon exposure to energetic electrons. The initial step in the reaction was found to be the cleavage of the oxygen–hydrogen (reaction (1)) or carbon–hydrogen (reaction (2) and (3)) bonds upon decomposition of water, methane, and a generic hydrocarbon, respectively. The released hydrogen atoms have excess kinetic energy of a few electron volts (eV) and can overcome the barrier of addition to carbon monoxide (CO) of 0.12 eV and to carbon dioxide (CO<sub>2</sub>) of 1.10 eV forming the formyl (HCO) and *trans*-hydroxycarbonyl (HOCO) radical, respectively (reactions (4) and (5)). If the geometry is favorable, barrier-less radical–radical recombinations lead to the formation of formic acid (6), acetic acid (7), and alkyl-carboxylic acids (8) at 10 K within the ices.



In analogy to these processes, the pyridine molecule can fragment upon exposure to ionizing radiation via carbon–hydrogen loss to *o*-, *m*-, and *p*-pyridinyl radicals plus atomic hydrogen (reaction (9)), followed by reaction (5) with the suprathreshold hydrogen atom, and recombination of the pyridinyl with the hydroxycarbonyl radical (reaction (10)). Although not yet identified in interstellar ices, pyridine may be formed in cold molecular clouds via the reaction of the cyano radical (CN) with 1,3-butadiene (C<sub>4</sub>H<sub>6</sub>) [23,24]. During the lifetime of a molecular cloud of 10<sup>5</sup>–10<sup>6</sup> years, pyridine could condense on the interstellar grains at concentrations below the detection limit of a few percent.



Smith et al. [25] attempted to emulate these conditions in laboratory experiments by exposing a series of pyridine–carbon dioxide and pyridine–carbon dioxide–water ices in a high vacuum chamber with pressures of a few 10<sup>−7</sup> torr to energetic protons resulting in the formation of pyridine mono- (*o*-, *m*-, *p*-) and disubstituted (2,3-, 3,4-, and 3,5-) carboxylic acids as identified ex situ through mass spectroscopy utilizing a direct analysis in real time (DART-MS) ion source and liquid chromatography coupled with UV detection and orbitrap mass spectrometry (LC–UV/MS). However, the off-line detection of the carboxylic acids raises the question if these molecules were formed within interstellar model ices and/or as a result of the hydrolysis of the extracted residues at room temperature by the solvent (water–methanol) thus making it impossible to define the source of the pyridine carboxylic acids, i.e. do these acids originate from their monomers or do they resemble hydrolysis products from the polymeric residue.

Here we explore the formation of pyridine carboxylic acids in interstellar ices analogs following irradiation with energetic electrons at 10 K on line and in situ. In contrast to previous studies, our experiments were conducted under contamination-free ultra-high vacuum conditions with pressures of 10<sup>−11</sup> torr; further, the data collection was carried out on line and in situ thus preventing contamination and hydrolysis of any residues. Furthermore, the on line studies enabled us to conduct mechanistical studies on the

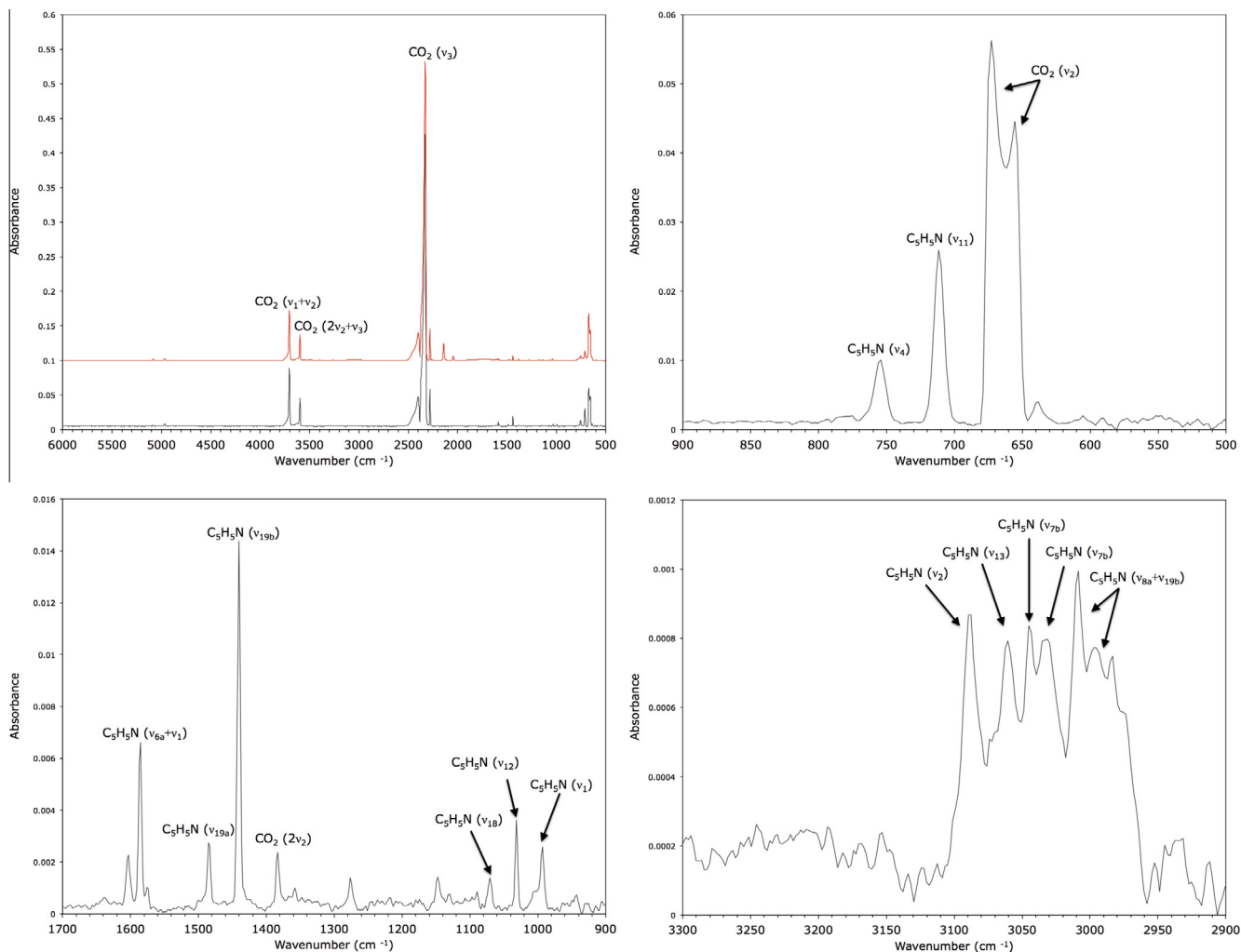


**Fig. 2.** Mid-infrared spectra of the solid 10% pyridine ( $C_5H_5N$ ) in carbon dioxide ( $CO_2$ ) ice before the irradiation at 10 K (black). The top left spectrum displays the full spectral range of 6000–500  $cm^{-1}$  with the irradiated ice shown in red. The remaining three panels depict zoomed in regions of the full spectrum. The assignment of peaks corresponding to the two starting materials is displayed on each graph. (For interpretation of the references to colour in this figure legend, the reader is referred to the web version of this article.)

formation mechanism(s) of these carboxylic acids along with corresponding rate constants.

## 2. Experimental

The experiments were carried out in a contamination-free, ultra-high vacuum (UHV) chamber evacuated to a pressure of  $5 \times 10^{-11}$  Torr [26,27]. Desired ultrahigh vacuum conditions were achieved through the utilization of a magnetically suspended turbo-pump (Osaka TG420MCAB) backed by an oil-free scroll pump (Anest Iwata ISP-500). A highly polished silver wafer attached to an oxygen free high conductivity (OFHC) copper target interfaced to a two-stage closed-cycle helium refrigerator and programmable temperature controller capable of regulating temperatures between 10 and 330 K was placed at the center of the chamber [28]. The premixed gas mixture of pyridine–carbon dioxide was prepared by mixing 10 mbar of pyridine vapor ( $C_5H_5N$ , Sigma Aldrich, 99.8+%) and 90 mbar carbon dioxide ( $CO_2$ , Airgas, 99.999%) into an evacuated gas mixing chamber. The pyridine used for this experiment was purified by triply freezing with liquid nitrogen and evacuating the headspace, thus removing gaseous impurities such as nitrogen and oxygen. The deposition of the ice was controlled by leaking the gas mixture through a precision leak valve and glass capillary

array for 25 min at 10 K at a pressure of  $5 \times 10^{-8}$  torr into the main chamber. The thickness of the ice was determined to be  $540 \pm 80$  nm. Here, the ice thickness was determined in situ via laser interferometry [29,30] with two helium–neon (HeNe) lasers operating at 632.8 nm. Computation of the thickness also required a value for the index of refraction for the ice mixture, to which the value for carbon dioxide ( $n_{CO_2} = 1.245$  [31]) was used based on the approximation that the ice composition closely resembled that of a pristine carbon dioxide ice. Relative abundance of the two starting materials was determined via a modified Beer–Lambert Law [26]. For carbon dioxide, the average column density was determined based on the integrated areas of  $\nu_1 + \nu_3$  and  $2\nu_2 + \nu_3$  of  $CO_2$  and  $\nu_3$  of  $^{13}CO_2$ , along with their corresponding absorption coefficients of  $1.4 \times 10^{-18}$   $cm$  molecule $^{-1}$ ,  $4.5 \times 10^{-19}$   $cm$  molecule $^{-1}$ , and  $7.8 \times 10^{-17}$   $cm$  molecule $^{-1}$ , respectively [32]. From this, the average column density of carbon dioxide in the ice mixture was found to be  $(2.64 \pm 0.08) \times 10^{17}$  molecule  $cm^{-2}$ . After taking into account the solid density of carbon dioxide ( $0.98$   $g$   $cm^{-3}$  [33]) the average thickness of the carbon dioxide component was determined to be  $480 \pm 30$  nm, translating to a relative abundance of approximately 8:1 ( $CO_2/C_5H_5N$ ).

Fig. 2 depicts the infrared spectrum of the deposited ice prior to the irradiation recorded with a Nicolet 6700 FTIR Spectrometer

**Table 1**  
Assignment of vibrational modes in pristine pyridine–carbon dioxide ice ( $C_5H_5N-CO_2$ ) at 10 K.

Absorption ( $cm^{-1}$ )	Literature value ( $cm^{-1}$ )	Assignment	Characterization
5085, 4967, 4828	...	$CO_2$	Combinations and Overtones
3710	3700 <sup>a</sup>	$\nu_1 + \nu_3 CO_2$	Combination
3600	3600 <sup>a</sup>	$2\nu_2 + \nu_3 CO_2$	Combination
3089	3087 <sup>b</sup>	$\nu_2 C_5H_5N$	C–H stretch
3062	3061 <sup>b</sup>	$\nu_{13} C_5H_5N$	C–H stretch
3044	3042 <sup>b</sup>	$\nu_{7b} C_5H_5N$	C–H Stretch
3034	3030 <sup>b</sup>	$\nu_{20a} C_5H_5N$	C–H stretch
3009, 2995	3010 <sup>b</sup>	$\nu_{8a} + \nu_{19b} C_5H_5N$	Combination
2430	2429 <sup>b</sup>	$\nu_{14} + \nu_{18a} C_5H_5N$	Combination
2328	2342 <sup>a</sup>	$\nu_3 CO_2$	Asymmetric stretch
2280	2282 <sup>a</sup>	$\nu_3 {}^{13}CO_2$	Asymmetric stretch
2044	2040 <sup>b</sup>	$\nu_{6a} + \nu_{19b} C_5H_5N$	Combination
1938	1925 <sup>b</sup>	$\nu_{9a} + \nu_{11} C_5H_5N$	Combination
1639	1641 <sup>b</sup>	$\nu_{11} + \nu_1 C_5H_5N$	Combination
1603	1598 <sup>b</sup>	$\nu_{6a} + \nu_1 C_5H_5N$	Combination
1585, 1574	1581 <sup>b</sup>	$\nu_{8a} C_5H_5N$	Ring stretch
1484	1483 <sup>b</sup>	$\nu_{19a} C_5H_5N$	Ring stretch
1441	1442 <sup>b</sup>	$\nu_{19b} C_5H_5N$	Ring stretch
1383	1384 <sup>a</sup>	$2\nu_2 CO_2$	Overtone
1358	1362 <sup>b</sup>	$\nu_{14} C_5H_5N$	Ring stretch
1276	1276 <sup>a</sup>	$\nu_1 CO_2$	Symmetric stretch
1147	1143 <sup>b</sup>	$\nu_{15} C_5H_5N$	C–H deform
1071	1071 <sup>b</sup>	$\nu_{18a} C_5H_5N$	C–H deform
1032	1032 <sup>b</sup>	$\nu_{12} C_5H_5N$	Trigonal ring breathing
993	991 <sup>b</sup>	$\nu_1 C_5H_5N$	Ring breathing
755	744 <sup>b</sup>	$\nu_4 C_5H_5N$	Ring twist
711	700 <sup>b</sup>	$\nu_{11} C_5H_5N$	C–H out-of-plane deform
673, 655	667, 665 <sup>a</sup>	$\nu_2 CO_2$	In-plane/out-of-plane bend
638	638 <sup>a</sup>	$\nu_2 {}^{13}CO_2$	In-plane/out-of-plane bend

<sup>a</sup> Bennett et al. [34].

<sup>b</sup> Wong et al. [35].

(reflection angle  $\alpha = 75^\circ$  [20]) along with vibrational assignments based upon literature values [35,36]. The assigned bands allude to the deposition of a composite ice film, with vibrations corresponding to pyridine and carbon dioxide present. Most notably, the  $\nu_1 + \nu_3$ ,  $\nu_3$ , and  $\nu_2$  absorptions of carbon dioxide, present at 3750–3690, 2500–2300, and 700–650  $cm^{-1}$ , respectively, correspond closely to interstellar model ices studied by Bennett et al. [36]. Likewise, evidence for C–H stretching and ring modes of pyridine are apparent in the 3100–2950 and 1370–1000  $cm^{-1}$  regions, respectively, aligning with literature values of solid-state pyridine [35] (Table 1). The ice was then irradiated for 60 min with 5 keV electrons at a current of 100 nA from a Specs EQ 22–35 electron gun. The electron beam exposed an area of  $3.2 \pm 0.3 cm^2$  at an angle of  $15^\circ$  relative to the surface normal with an actual extraction efficiency of 78.8% of the electrons by scanning the beam over the ice surface. The electron trajectories and energy transfer inside the ices was modeled by the CASINO program [37]. These simulations yielded an imparted energy of  $4.7 \pm 0.5 keV$  per electron at an average penetration depth of  $390 \pm 20 nm$  (less than the thickness of the ice to avoid interaction of the electrons with the silver wafer) translating to an average of  $4.0 \pm 0.1 eV$  absorbed per molecule in the deposited ice. This value corresponds to an average linear energy transfer (LET) of  $12 keV \mu m^{-1}$ , on the order of magnitude 10–20 MeV cosmic rays transfer to interstellar ices [38,39]. The

irradiated ice remained at 10 K for an additional 60 min before being heated to 293 K at a rate of 0.5  $K min^{-1}$ . In situ FTIR data were collected throughout the irradiation and temperature programmed desorption (TPD) protocol. Mass spectra (Balzers QMG 422 Quadrupole Mass Spectrometer) were collected up to a mass-to-charge ratio of  $m/z = 200$  using an electron impact ionization energy of 100 eV at an emission current of 0.2 mA to monitor gaseous species released during the TPD phase [40,41].

### 3. Results

#### 3.1. Infrared spectroscopy

##### 3.1.1. Qualitative analysis

Evidence for the radiation-induced formation of new species in the binary ices is apparent by novel bands present in the post-irradiation ice mixture at 10 K. Due to the newly formed carboxylic acid species not desorbing during the TPD phase, QMS data failed to indicate the formation of these species. However, volatile reactants and light carbon species – such as carbon monoxide (CO) and carbon dioxide ( $CO_2$ ) – were monitored to determine the temperature of desorption. The absorption features were deconvoluted exploiting Gaussian fits (Fig. 3) utilizing the peak fitting application on GRAMS-AI. Details on the algorithm employed by GRAMS-AI for fittings are described in Press et al. [42]. Peaks were iteratively fit to spectra so that the residual of the unfit portion was equivalent to the baseline noise. In situ spectra throughout the warm-up period are presented to display bands resulting from radiation products present following the sublimation of the volatile reactants. Particular interest is directed to those spectral regions associated with peaks characteristic to pyridine carboxylic acids and the proposed reactive intermediate, the HOCO radical. The novel absorption features along with the literature assignments are summarized in Table 2. A comprehensive summary of literature values for all pyridine carboxylic acid species along with the corresponding bands observed in this study is provided in Tables 3 and 4.

The newly emerging bands found within the electron-irradiated ice are indicative of the formation of a variety of pyridine carboxylic acids along with the hydroxycarbonyl (HOCO) radical, carbon trioxide ( $CO_3$ ), carbon monoxide (CO) at 2141  $cm^{-1}$ , and ozone ( $O_3$ ) at 1032  $cm^{-1}$ . We were able to identify the HOCO radical based on the absorption at 1845  $cm^{-1}$  corresponding to the  $\nu_2$  (CO) stretching mode. These assignments are in agreement with previous studies of the HOCO radical in an argon matrix at 1846  $cm^{-1}$  [43] and as a byproduct of electron irradiation of interstellar model ices composed of carbon dioxide ( $CO_2$ )–hydrocarbon ( $C_nH_{2n+2}$ ;  $n = 1–6$ ) and methanol ( $CH_3OH$ )–carbon monoxide (CO) both at 1852  $cm^{-1}$  [21,41].

The processed ice at 10 K also displayed unambiguous evidence for the formation of the biologically relevant nicotinic acid ( $m-C_5H_4NCOOH$ ) based on a peak at 1555  $cm^{-1}$  ( $\nu_8$  [ring stretch]). This observed band agrees closely with a study completed on nicotinic acid in potassium bromide (KBr) pellets which assigned  $\nu_8$  at 1540  $cm^{-1}$  [44]. Additionally, 2,5-, 3,4-, and 3,5-pyridine dicarboxylic acid ( $C_5H_3N(COOH)_2$ ) were identified unambiguously based on their bands at 1775  $cm^{-1}$  ( $\nu(C=O)$ ), 1638  $cm^{-1}$  ( $\nu(\text{ring})$ ), and 1359  $cm^{-1}$  ( $\nu_{33}$  [ring stretch]), respectively. The 2,5- and 3,4- species were assigned to their respective carriers on the basis of a study conducted on the full suite of solid pyridine dicarboxylic acids in KBr. The two aforementioned vibrations are unique to the 2,5- and 3,4- isomers, exhibiting literature bands at 1770  $cm^{-1}$  and 1640  $cm^{-1}$  [45], respectively. Likewise, Nataraj et al. [46] in the study of 3,5-pyridine dicarboxylic acid in KBr found  $\nu_{33}$  to occur at 1357  $cm^{-1}$ , matching the peak observed within this study.

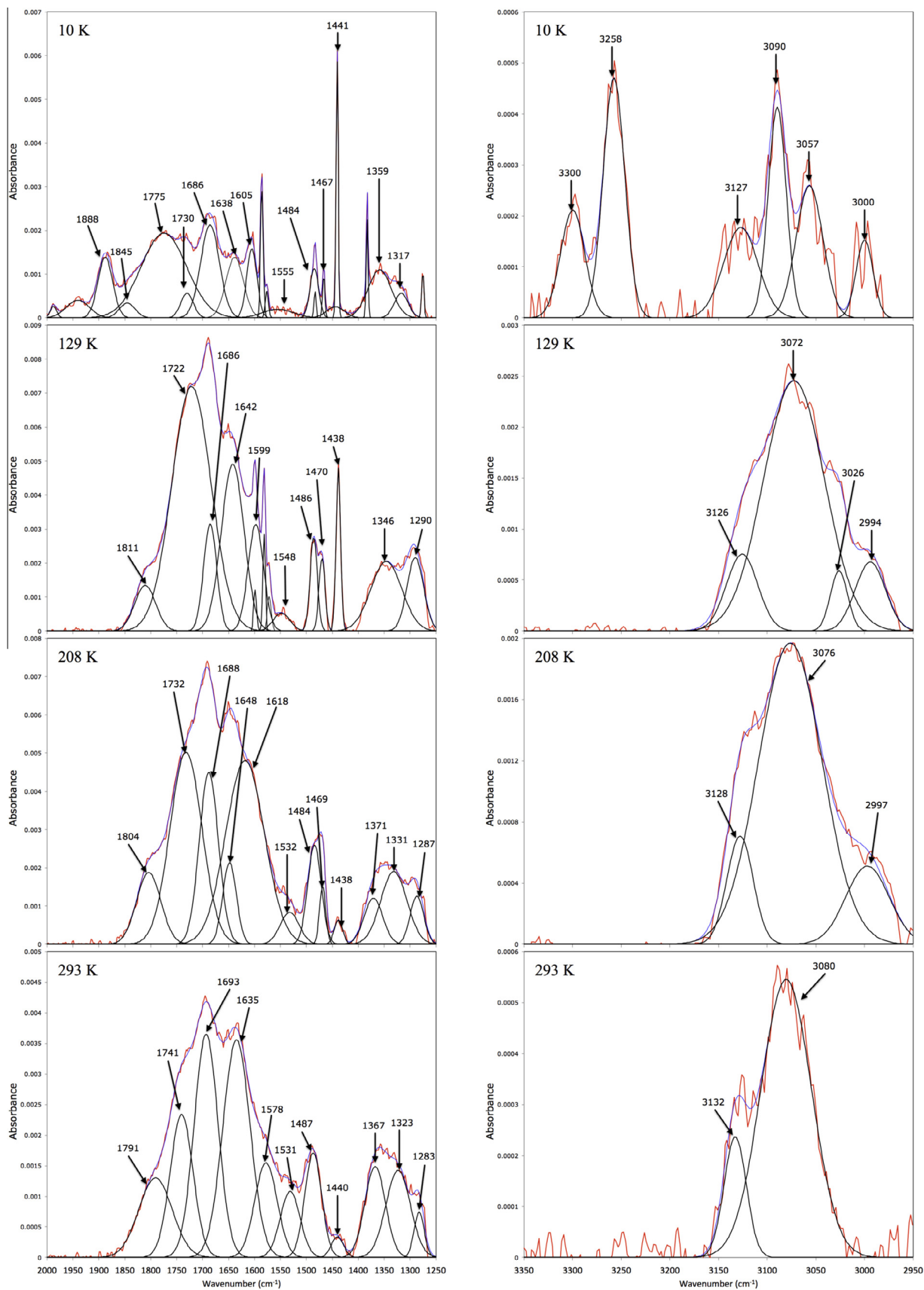


**Fig. 3.** Deconvoluted infrared spectrum of ice following irradiation with energetic electrons at 10 K, 129 K, 208 K, and 293 K (from top to bottom). The two regions in which relevant bands were found, 3350–2950 cm<sup>-1</sup> (left) and 1950–1400 cm<sup>-1</sup> (right), are displayed. The red lines correspond to experimentally collected infrared spectra, the black lines correspond to deconvoluted fits of structures within the ice, and the blue line corresponds to the sum of the deconvoluted fittings. Absorption features assigned to radiation products are labeled by wavenumber. (For interpretation of the references to colour in this figure legend, the reader is referred to the web version of this article.)

**Table 2**  
Infrared absorption features of the irradiated pyridine–carbon dioxide ice ( $C_5H_5N-CO_2$ ) at 10 K and throughout heating period.

Absorptions after irradiation <sup>a</sup> 10 K	Absorptions during warm-up <sup>a</sup>			Literature assignment			
	129 K	208 K	293 K	Wavenumber ( $cm^{-1}$ )	Molecule	Vibration	Characterization
2141	–	–	–	2139 <sup>b</sup>	CO	$\nu_1$	Fundamental
2044	–	–	–	2041 <sup>b</sup>	$CO_3$	$\nu_1$	C–O stretch
1888	–	–	–	1879 <sup>b</sup>	$CO_3$	–	Fermi resonance
1845	–	–	–	1846 <sup>c</sup>	HOCO	$\nu_2$	C–O stretch
–	1811	1804	1791	1790 <sup>d</sup>	$2,5-C_5H_3N(COOH)_2$	–	C–O stretch
1775	–	–	–	1770 <sup>d</sup>	$2,5-C_5H_3N(COOH)_2$	–	C–O stretch
1730	1722	1732	1741	1730 <sup>d</sup>	$2,4-C_5H_3N(COOH)_2$	–	C–O stretch
–	–	–	–	1730 <sup>d</sup>	$2,5-C_5H_3N(COOH)_2$	–	C–O stretch
1686	1686	1688	1693	1700 <sup>e</sup>	$2,6-C_5H_3N(COOH)_2$	–	C–O stretch
–	–	–	–	1704 <sup>f</sup>	$3,4-C_5H_3N(COOH)_2$	$\nu_6$	C–O stretch
1638	1642	1648	1635	1640 <sup>f</sup>	$3,4-C_5H_3N(COOH)_2$	–	Ring stretch
1605	1599	1618	1578	1595 <sup>g,h</sup>	$o-C_5H_4NCOOH$	$\nu_{8a}$	Ring stretch
–	–	–	–	1595 <sup>h</sup>	$m-C_5H_4NCOOH$	–	Ring stretch
–	–	–	–	1610 <sup>d</sup>	$2,3-C_5H_3N(COOH)_2$	–	Ring stretch
–	–	–	–	1590 <sup>d</sup>	$2,4-C_5H_3N(COOH)_2$	–	Ring stretch
–	–	–	–	1610 <sup>d</sup>	$2,5-C_5H_3N(COOH)_2$	–	Ring stretch
–	–	–	–	1609 <sup>d</sup>	$3,4-C_5H_3N(COOH)_2$	$\nu_8$	Ring stretch
–	–	–	–	1597 <sup>i</sup>	$3,5-C_5H_3N(COOH)_2$	$\nu_{37}$	Ring stretch
1555	1548	1532	1531	1540 <sup>i</sup>	$m-C_5H_4NCOOH$	$\nu_8$	Ring stretch
1485	1486	1484	1487	1488 <sup>h</sup>	$m-C_5H_4NCOOH$	–	Ring stretch
–	–	–	–	1480 <sup>d</sup>	$2,3-C_5H_3N(COOH)_2$	–	Ring stretch
1467	1470	1469	–	1478 <sup>h</sup>	$p-C_5H_4NCOOH$	–	Ring stretch
–	–	–	–	1470 <sup>d</sup>	$2,5-C_5H_3N(COOH)_2$	–	Ring stretch
–	–	–	–	1470, 1468 <sup>e</sup>	$2,6-C_5H_3N(COOH)_2$	–	CH wag, ring stretch
1441	1438	1438	1440	1439 <sup>g,h</sup>	$o-C_5H_4NCOOH$	$\nu_{19b}$	Ring stretch
–	–	–	–	1440 <sup>h,j</sup>	$m-C_5H_4NCOOH$	$\nu_9$	Ring stretch
–	–	–	–	1443 <sup>i</sup>	$3,5-C_5H_3N(COOH)_2$	$\nu_{35}$	Ring stretch
1359	1346	1371	1367	1357 <sup>i</sup>	$3,5-C_5H_3N(COOH)_2$	$\nu_{33}$	Ring stretch
1317	–	1331	1323	1325 <sup>i</sup>	$m-C_5H_4NCOOH$	$\nu_{10}$	In-plane (COH) def
–	–	–	–	1317 <sup>f</sup>	$3,4-C_5H_3N(COOH)_2$	$\nu_{14}$	Ring stretch
–	1290	1287	1283	1280 <sup>d</sup>	$2,3-C_5H_3N(COOH)_2$	–	OH scissor
1032	1032	–	–	1037 <sup>k</sup>	$O_3$	$\nu_3$	Asymmetric stretch

<sup>a</sup> Only new absorption features and those present in ice at 298 K are reported as product peaks; carbon dioxide ( $CO_2$ ) and other light carbon species sublimed prior to 70 K, leaving pyridine ( $C_5H_5N$ ) and heavier radiation products; pyridine ( $C_5H_5N$ ) sublimed prior to 109 K, leaving only heavy radiation products.

<sup>b</sup> Bennett et al. [26].

<sup>c</sup> Jacox [43].

<sup>d</sup> Wasylyna et al. [45].

<sup>e</sup> Massaro et al. [47].

<sup>f</sup> Karabacak et al. [48].

<sup>g</sup> Lewandowski et al. [49].

<sup>h</sup> Koczoń et al. [50].

<sup>i</sup> Nataraj et al. [46].

<sup>j</sup> Kumar et al. [44].

<sup>k</sup> Bennett et al. [51].

In our experiments we also observed the infrared spectra of the ices throughout the TPD phase. In the irradiated ice at 129 K we observe new bands at  $1811\text{ cm}^{-1}$  and  $1290\text{ cm}^{-1}$ . From a previously mentioned study on pyridine dicarboxylic acids [45] we find that the band at  $1811\text{ cm}^{-1}$  can be unambiguously assigned to the carrier 2,5-pyridine dicarboxylic acid due to its close resemblance with the literature value of  $1790\text{ cm}^{-1}$ . The same study confirms the peak at  $1290\text{ cm}^{-1}$  as  $\sigma(\text{OH})$  of 2,3-pyridine dicarboxylic acid based on the published value of  $1280\text{ cm}^{-1}$ .

### 3.1.2. Quantitative analysis

Utilizing the peak assignments from Section 3.1.1, a decrease in the column densities of the reactants, pyridine and carbon dioxide, can be computed along with the yields of the radiation products (Fig. 4). For carbon dioxide, the temporal evolution of the  $\nu_1 + \nu_3$  and  $2\nu_2 + \nu_3$  of  $CO_2$  and  $\nu_3$  of  $^{13}CO_2$  were monitored to determine the quantity of carbon dioxide molecules destroyed. We determined that  $(3.4 \pm 0.9) \times 10^{16}$  molecule  $cm^{-2}$  carbon dioxide

were degraded exploiting integrated absorption coefficients of  $1.4 \times 10^{-18}$  cm molecule $^{-1}$ ,  $4.5 \times 10^{-19}$  cm molecule $^{-1}$ , and  $7.8 \times 10^{-17}$  cm molecule $^{-1}$  for  $\nu_1 + \nu_3$  and  $2\nu_2 + \nu_3$  of  $CO_2$  and  $\nu_3$  of  $^{13}CO_2$ , respectively. With the diminishing column density of carbon dioxide, new absorption features corresponding to carbon monoxide and carbon trioxide were observed. Formation of the two new carbon oxide species was monitored based on the fundamental band of carbon monoxide, present at  $2141\text{ cm}^{-1}$ , and the  $\nu_1$  of carbon dioxide at  $2044\text{ cm}^{-1}$ . Bennett et al. [26] defined the integrated absorption coefficients of the two aforementioned bands as  $1.1 \times 10^{-17}$  cm molecule $^{-1}$  and  $3.1 \times 10^{-17}$  cm molecule $^{-1}$ , respectively. We find that over the course of the irradiation, the total increase in column density of carbon monoxide was  $(9.3 \pm 0.8) \times 10^{15}$  molecule  $cm^{-2}$ , while the total increase of carbon trioxide was  $(6.2 \pm 0.2) \times 10^{14}$  molecule  $cm^{-2}$ . Additionally, marginal yields of the HOCO radical were recognized by the band at  $1845\text{ cm}^{-1}$  corresponding to its  $\nu_2$  band. Based on its integrated absorption coefficient of  $3.6 \times 10^{-17}$  cm molecule $^{-1}$  [17], the

**Table 3**

Infrared absorption features of the irradiated pyridine–carbon dioxide ice ( $C_5H_5N-CO_2$ ) at 10 K and throughout heating period compared to literature values for mono- and disubstituted pyridine carboxylic acids.

Experimental absorptions ( $cm^{-1}$ ) <sup>a</sup> 10 K	Literature values ( $cm^{-1}$ )								
	Monosubstituted			Disubstituted					
	<i>Ortho</i> - <sup>b,c</sup>	<i>Meta</i> - <sup>c,d</sup>	<i>Para</i> - <sup>c</sup>	2,3- <sup>e</sup>	2,4- <sup>e</sup>	2,5- <sup>e</sup>	2,6- <sup>f</sup>	3,4- <sup>e,g</sup>	3,5- <sup>h</sup>
1811–1790	...	...	...	...	...	1790	...	...	...
1775	...	...	...	...	...	1770	...	...	...
1741–1722	...	...	...	...	1730	1730	...	...	...
...	1717	1711 1708	1712	...	...	...	1710	1704	...
1693–1686	...	...	...	...	...	...	1700	...	...
1648–1635	...	...	...	...	...	...	...	1640	...
...	1608	...	...	...	...	...	...	...	...
1618–1578	1595	1595 1583	1616 1597	1610 1580	1590	1610	1576	1609	1597
...	1573	...	...	...	...	...	1571	...	...
1548–1531	...	1540	...	...	...	...	...	...	...
...	...	...	...	...	1500	...	...	...	...
1487–1484	...	1488	...	1480	...	...	...	...	...
...	...	...	1478	...	...	...	...	...	...
1470–1467	...	...	...	...	...	1470	1470 1468	...	...
...	1455	...	...	...	...	...	...	...	...
1441–1438	1439	1440	...	...	...	...	...	...	1443
...	...	1407	1412	1430 1420	1390	1420 1400	1422 1387	1405	1383
1371–1346	...	...	...	...	...	...	...	...	1357
...	...	...	...	...	...	...	1341	...	...
1331–1317	...	1325	...	...	...	...	...	1317	...
...	...	...	...	1310	1310	...	1308	...	1298
1290–1283	...	...	...	1280	...	...	...	...	...

<sup>a</sup> Range of wavenumbers indicates the shift in the assigned band between the irradiated sample at 10 K and during the warm-up.

<sup>b</sup> Lewandowski et al. [49].

<sup>c</sup> Koczoń et al. [50].

<sup>d</sup> Kumar et al. [52].

<sup>e</sup> Wasylińska et al. [45].

<sup>f</sup> Massaro et al. [47].

<sup>g</sup> Karabacak et al. [48].

<sup>h</sup> Nataraj et al. [46].

column density of the HOCO radical in the irradiated ice was  $(7.3 \pm 0.9) \times 10^{13}$  molecule  $cm^{-2}$ . The total column density of newly formed carbon dioxide-based products is therefore computed to be  $(1.0 \pm 0.1) \times 10^{16}$  molecule  $cm^{-2}$ , i.e.  $29 \pm 9\%$  of the destroyed carbon dioxide was transformed into carbon trioxide, carbon monoxide, and the hydroxycarbonyl radical. We conclude that the difference between the amount of carbon dioxide destroyed and the column density of these newly formed light carbon species must be the column density of carbon dioxide molecules incorporated into pyridine carboxylic acids:  $(2.4 \pm 0.9) \times 10^{16}$  molecule  $cm^{-2}$ .

For pyridine, the change in column density is determined by monitoring the temporal development of its  $\nu_4$  and  $\nu_{11}$  bands at  $755\text{ cm}^{-1}$  and  $711\text{ cm}^{-1}$ , respectively, using integrated absorption coefficients of  $8.3 \times 10^{-19}$   $cm\text{ molecule}^{-1}$  and  $2.4 \times 10^{-18}$   $cm\text{ molecule}^{-1}$ . Based on the initial column density of pyridine in the pristine ice and the change in peak area of the aforementioned bands, an average of  $(1.6 \pm 0.2) \times 10^{16}$  molecule  $cm^{-2}$  pyridine molecules were destroyed over the course of the irradiation. Since no other carriers containing the pyridine moiety were identified in the processed ice, it can be concluded that all the destroyed pyridine molecules were converted to pyridine carboxylic acids. Therefore, we establish an upper limit for the pyridine carboxylic acid column density to be  $(1.6 \pm 0.2) \times 10^{16}$  molecule  $cm^{-2}$ , incorporating  $6 \pm 2\%$  of the carbon dioxide reactant molecules. Completion of the mass balance for the irradiated ice involves determining

the average number of carboxyl groups incorporated into each newly formed pyridine carboxylic acid. Based on the proposed reaction mechanism outlined by reactions (5), (9), and (10), it is determined the average number of carboxyl groups is equal to the column density of destroyed carbon dioxide divided by the upper limit of the carboxylic acid column density. In this manner, we find that an average of about 1.5 carbon dioxide molecules were consumed per pyridine carboxylic acid molecule formed, implying a near equal mixture of mono- and disubstituted pyridine molecules in the processed ice. These findings are consistent with the assignment of a suite of mono- and disubstituted pyridine carboxylic acid species within the irradiated ice as outlined above.

#### 4. Discussion

Having assigned the carriers of the newly formed molecules within the irradiated pyridine–carbon dioxide ice, we attempt now to elucidate the reaction mechanism involved in the production of the identified pyridine carboxylic acids. Similar to the mechanisms extracted in previous studies of carboxylic acid formation in interstellar model ices [21,39], the initial step in the formation of pyridine carboxylic acids in this study is the loss of a hydrogen atom, as described in reaction (9), from pyridine. This reaction is essentially a carbon–hydrogen bond cleavage and is highly endogenic by  $439\text{ kJ mol}^{-1}$  (4.55 eV) for the *o*-pyridinyl radical and by  $468\text{ kJ mol}^{-1}$  (4.85 eV) for the *m*- and *p*-pyridinyl

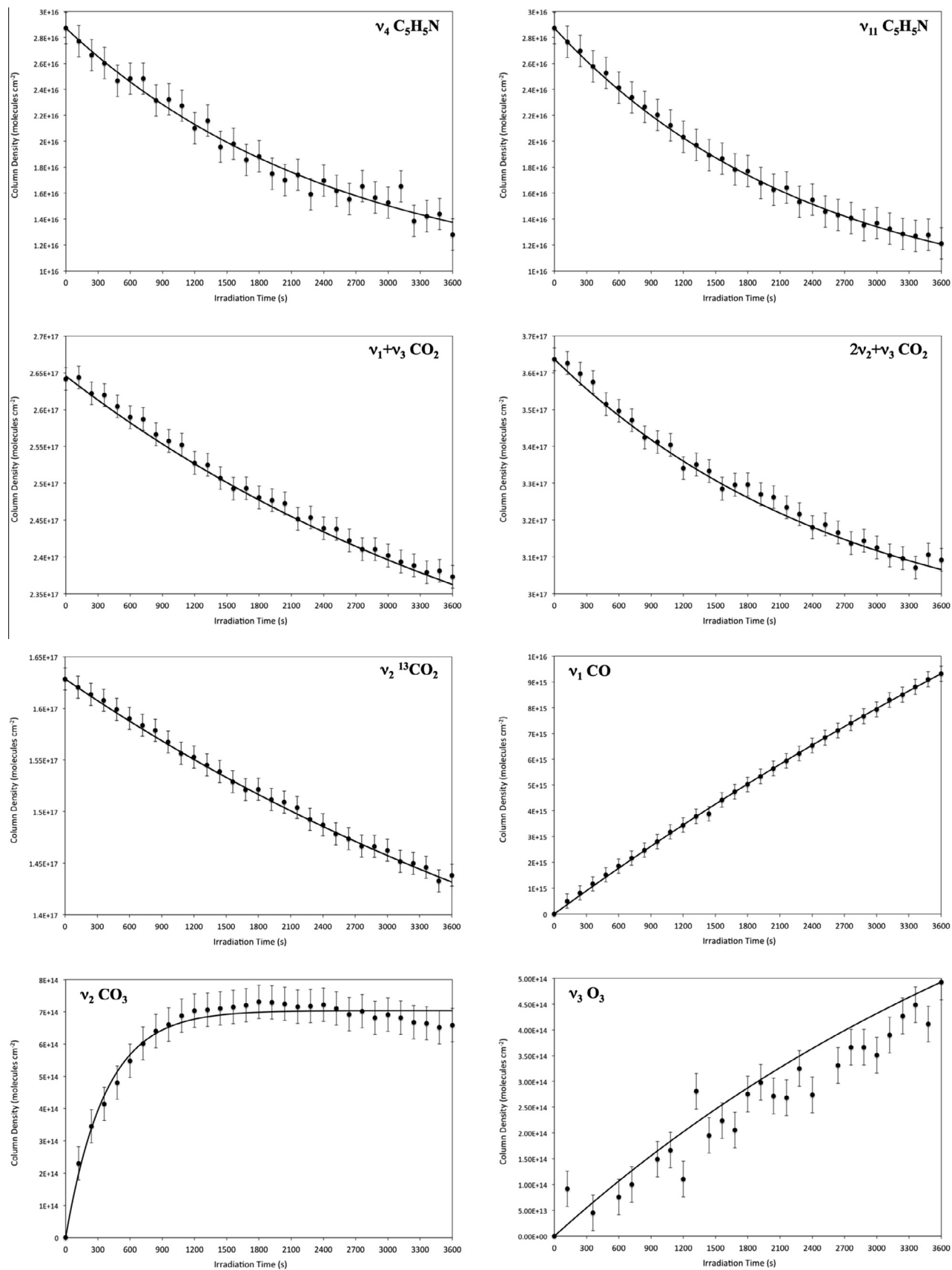


**Fig. 4.** Fit of temporal (integrated IR absorption) evolution of the two starting materials pyridine (C<sub>5</sub>H<sub>5</sub>N) and carbon dioxide (CO<sub>2</sub>), and the newly formed light irradiation products carbon monoxide (CO), carbon trioxide (CO<sub>3</sub>), and ozone (O<sub>3</sub>) throughout the 1-h irradiation period.

**Table 4**

Compilation of new molecules formed in pyridine–carbon dioxide ice ( $C_5H_5N-CO_2$ ) at 10 K and throughout heating period.

Molecule	Absorption ( $cm^{-1}$ ) <sup>a</sup>	Literature value ( $cm^{-1}$ )	Assignment
<i>o</i> - $C_5H_4NCOOH$	1618–1578	1595 <sup>b,c</sup>	$\nu_{8a}$
	1441–1438	1439 <sup>b,c</sup>	$\nu_{19b}$
<i>m</i> - $C_5H_4NCOOH$	1618–1578	1595, 1583 <sup>c,d</sup>	$\nu(\text{ring})$
	1548–1531	1540 <sup>d</sup>	$\nu_8$
	1487–1484	1488 <sup>d</sup>	$\nu(\text{ring})$
	1441–1438	1440 <sup>c,d</sup>	$\nu_9$
	1331–1317	1325 <sup>d</sup>	$\nu_{10}$
<i>p</i> - $C_5H_4NCOOH$	1618–1578	1616, 1597 <sup>c</sup>	$\nu(\text{ring})$
2,3- $C_5H_3N(COOH)_2$	1618–1578	1610, 1580 <sup>e</sup>	$\nu(\text{ring})$
	1487–1484	1480 <sup>e</sup>	$\nu(\text{ring})$
	1290–1283	1280 <sup>e</sup>	$\sigma(\text{OH})$
2,4- $C_5H_3N(COOH)_2$	1741–1722	1730 <sup>e</sup>	$\nu(\text{C-O})$
	1618–1578	1590 <sup>e</sup>	$\nu(\text{ring})$
2,5- $C_5H_3N(COOH)_2$	1811–1790	1790 <sup>e</sup>	$\nu(\text{C-O})$
	1775	1770 <sup>e</sup>	$\nu(\text{C-O})$
	1741–1722	1730 <sup>e</sup>	$\nu(\text{C-O})$
	1618–1578	1610 <sup>e</sup>	$\nu(\text{ring})$
	1470–1467	1470 <sup>e</sup>	$\nu(\text{ring})$
2,6- $C_5H_3N(COOH)_2$	1693–1686	1700 <sup>f</sup>	$\nu(\text{C-O})$
	1618–1578	1576 <sup>f</sup>	$\nu(\text{ring})$
	1470–1467	1470, 1468 <sup>f</sup>	$\rho(\text{CH}), \nu(\text{C-N})$
3,4- $C_5H_3N(COOH)_2$	1693–1686	1704 <sup>g</sup>	$\nu_6$
	1648–1635	1640 <sup>g</sup>	$\nu(\text{ring})$
	1618–1578	1609 <sup>g</sup>	$\nu_8$
	1331–1317	1317 <sup>g</sup>	$\nu_{14}$
3,5- $C_5H_3N(COOH)_2$	1618–1578	1597 <sup>h</sup>	$\nu_{37}$
	1441–1438	1443 <sup>h</sup>	$\nu_{35}$
	1371–1346	1357 <sup>h</sup>	$\nu_{33}$

<sup>a</sup> Range of wavenumbers indicates the shift in the assigned band between the irradiated sample at 10 K and during the warm-up.

<sup>b</sup> Lewandowski et al. [49].

<sup>c</sup> Koczoń et al. [50].

<sup>d</sup> Kumar et al. [44].

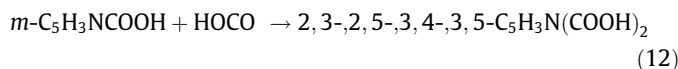
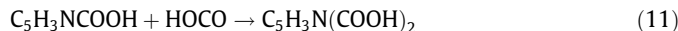
<sup>e</sup> Wasylińska et al. [45].

<sup>f</sup> Massaro et al. [47].

<sup>g</sup> Karabacak et al. [48].

<sup>h</sup> Nataraj et al. [46].

radicals [53]. The hydrogen atoms produced possess up to a few eV of kinetic energy [17,21]. Hydrogen atoms with sufficient kinetic energy are then capable of overcoming the entrance barrier of 106 kJ mol<sup>-1</sup> (1.10 eV) required to form the trans-carboxyl radical (HOCO (reaction (5))). These newly formed radicals undergo radical–radical recombination without barrier with the pyridinyl radical to form a monosubstituted pyridine carboxylic acid. In an analogous process, the monosubstituted carboxylic acids can lose a second hydrogen atom from the pyridine ring via interaction with energetic electrons to form a radical and an energetic hydrogen atom. These monosubstituted pyridine carboxylic acid radicals can then recombine with a hydroxycarbonyl (HOCO) radical – if the proper recombination geometry can be reached – to form a suite of disubstituted pyridine carboxylic acids (reaction (11)). As nicotinic acid (*m*- $C_5H_4NCOOH$ ) is the only monosubstituted species unambiguously assigned, we deduce it is the primary intermediate in the formation of the observed disubstituted acids: 2,3-, 2,5-, 3,4-, and 3,5- (reaction (12)). Due to the facile conversion of the hydroxycarbonyl (HOCO) radicals to carboxylic acids, the aforementioned reaction mechanism can be formally streamlined to reactions 13 and 14 (Fig. 5).

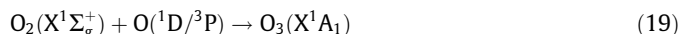
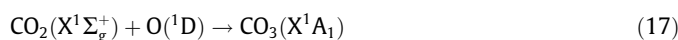
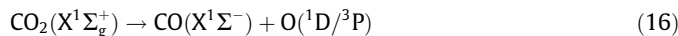


These reaction pathways were also verified by kinetically fitting the temporal evolution of the column densities (Table 5, Fig. 6). The temporal evolution of the observed pyridine carboxylic acids can be modeled by stepwise pathway A  $\rightarrow$  B  $\rightarrow$  C:

$$[C_5H_3N(COOH)_2]_t = a \left( 1 - \frac{k_2}{k_2 - k_1} e^{-k_1 t} - \frac{k_1}{k_2 - k_1} e^{-k_2 t} \right) \quad (15)$$

where  $k_1$  is the reaction rate of reaction (13) and  $k_2$  is the reaction rate of reaction (14). For this, the bands assigned to 2,5- and 3,4-pyridine carboxylic acids were monitored throughout the ice irradiation. Fig. 6 demonstrates the best fit of the two species where  $k_1 = (4.3 \pm 2.0) \times 10^{-4} \text{ s}^{-1}$  and  $k_2 = (2.7 \pm 1.2) \times 10^{-4} \text{ s}^{-1}$  for 2,5-pyridine carboxylic acid and  $k_1 = (4.5 \pm 1.7) \times 10^{-4} \text{ s}^{-1}$  and  $k_2 = (2.8 \pm 1.0) \times 10^{-4} \text{ s}^{-1}$  for 3,4-pyridine carboxylic acid. Collectively, we find that the addition of a single carbon dioxide molecule to pyridine proceeds forward with a rate constant of  $(4.4 \pm 2.6) \times 10^{-4} \text{ s}^{-1}$ , while the addition of a second carbon dioxide molecule to a mono-substituted species proceeds with a lower rate constant of  $(2.7 \pm 1.6) \times 10^{-4} \text{ s}^{-1}$ . The highly electronegative –COOH group likely reduces the rate of addition of a second hydroxycarbonyl radical.

As described in Section 3.1.2, the temporal profiles of carbon monoxide (CO), carbon trioxide (CO<sub>3</sub>), and ozone (O<sub>3</sub>) were also monitored throughout the irradiation. The following formation pathways (reactions (16)–(19)) are considered for the three aforementioned species:



Note that some of these reactions require intersystem crossing (ISC). Carbon dioxide is destroyed by reaction (16), producing a carbon monoxide molecule and an oxygen atom in the excited singlet state (<sup>1</sup>D) and/or triplet ground state (<sup>3</sup>P). This pathway is endoergic by 532 kJ mol<sup>-1</sup> (5.51 eV) for the triplet channel and by 732 kJ mol<sup>-1</sup> (7.59 eV) for the singlet channel. The energies required to complete these processes are provided by the energy deposited from energetic electrons passing through the ice mixture. Based on the electron fluence of  $5.5 \times 10^{14} \text{ electrons cm}^{-2}$ , each electron initiates the destruction of  $17 \pm 6$  carbon dioxide molecules, translating to  $90 \pm 30 \text{ eV electron}^{-1}$  or  $130 \pm 40 \text{ eV electron}^{-1}$  for the formation of ground and excited state oxygen atoms, respectively. These suprathreshold oxygen atoms react with unprocessed carbon dioxide to form carbon trioxide. Using a one step A'  $\rightarrow$  B' fitting (Eqs. (20) and (21)) the temporal profiles of carbon monoxide and carbon trioxide were modeled with the best fits displayed in Fig. 4.



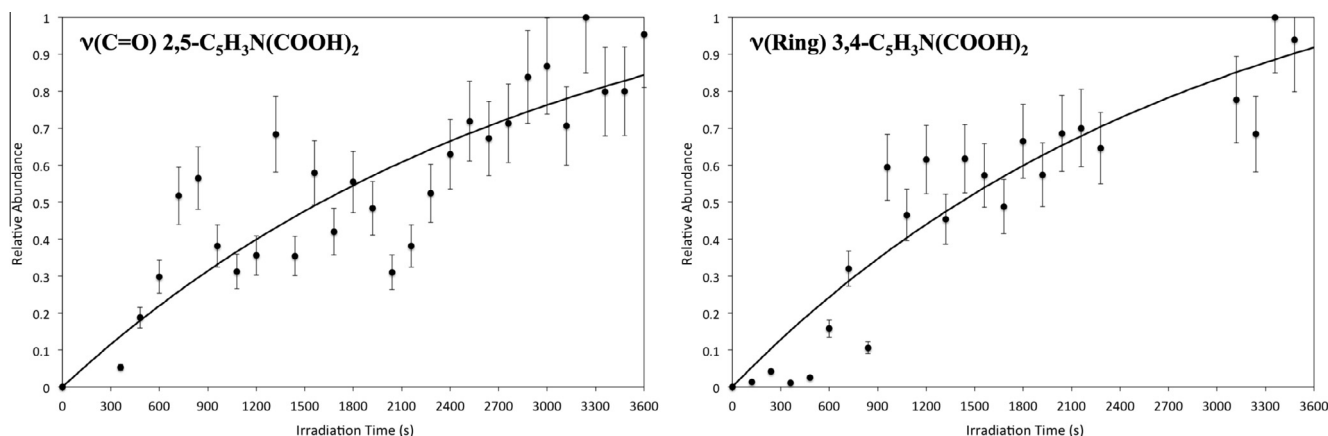


**Fig. 6.** Fit of temporal (normalized integrated IR absorption) evolution of 2,5- and 3,4-pyridine carboxylic acid throughout the 1-h irradiation period. The profiles were fit based on a pseudo first-order, consecutive  $\text{A} \rightarrow \text{B} \rightarrow \text{C}$  reaction scheme.

## 5. Conclusion

The present laboratory study demonstrates the formation of pyridine carboxylic acids, including the biologically relevant nicotinic acid (vitamin B3;  $m\text{-C}_5\text{H}_4\text{NCOOH}$ ) and four dicarboxylic acids (2,3-, 2,5-, 3,4-, and 3,5-), in icy mixtures of pyridine and carbon dioxide (1:8) upon exposure to ionizing radiation in the form of energetic electrons. The carboxylic acid species unambiguously characterized within this study align closely with those identified in the Murchison [1,2] and Tagish Lake [3] meteorites, i.e. all three monosubstituted pyridine carboxylic acids. Our findings also found a similar suite of pyridine carboxylic acids as a more recent investigation on a series of CM2-type carbonaceous chondrites [4] that detected all three monosubstituted and 2,5-, 3,4-, 3,5-pyridine carboxylic acids. Additionally, our study unambiguously identified the formation of the 2,3-dicarboxylic acid species. Collectively, the array of pyridine carboxylic acids formed in the present experiment mimics the result of previous studies focusing on the irradiation of pyridine-carbon dioxide and pyridine-carbon dioxide-water ice mixtures [4,25]. However, unlike the aforementioned study, our experiments were conducted under contamination-free ultrahigh vacuum conditions – more characteristic of interstellar environments – with infrared data collected on line and in situ – preventing the possibility of contamination or hydrolysis of the ice by solvents (water or water-methanol) needed for DART-MS and LC-UV/MS analysis. The on line nature of our study also allowed for analysis of the temporal evolution of irradiation products as identified by the development of novel bands throughout the processing period. Underlying reaction schemes for observed products were elucidated based on optimized fittings of the collected temporal profiles. It should be noted that this study is a proof-of-concept study to probe possible formation routes of pyridine carboxylic acids and further experiments with more characteristic interstellar ices, such as those including water ( $\text{H}_2\text{O}$ ), are necessary.

To model the formation of pyridine carboxylic acids mechanistically, laboratory experiments completed on the formation of generic alkyl carboxylic acids ( $\text{RCOOH}$ ) in interstellar model ices were referenced. Kim et al. [21] postulated that carboxylic acid formation is realized in hydrocarbon-carbon dioxide ice mixtures upon exposure to energetic electrons through the hydroxycarbonyl (HOCO) radical intermediate formed by reactions between carbon dioxide and suprathermal hydrogen atoms lost from a hydrocarbon,  $\text{R-H}$ . The alkyl and HOCO radical may then undergo radical-radical recombination to produce carboxylic acids. In an analogous process, we propose that pyridine upon interaction with ionizing

radiation may undergo hydrogen loss, followed by reaction of the latter with carbon dioxide leading to the formation of HOCO radical intermediates and subsequently pyridine carboxylic acids. Employing in situ infrared spectroscopy, the formation of radiation-induced mono- and disubstituted carboxylic acids was monitored along with the HOCO radical, and optimized kinetic fittings were obtained. From this, the rate constant for the addition of a single carboxyl group was determined to be  $(4.4 \pm 2.6) \times 10^{-4} \text{ s}^{-1}$ , comparable to the  $1.1 \times 10^{-4} \text{ s}^{-1}$  found for the formation of generic alkyl carboxylic acids in hydrocarbon-carbon dioxide ice mixtures [21]. Addition of a second carbon dioxide molecule to a monosubstituted pyridine carboxylic acid was found to proceed at a rate of  $(2.7 \pm 1.6) \times 10^{-4} \text{ cm}^2 \text{ s}^{-1}$ , slower than the initial addition of carbon dioxide to pyridine due to the effects of the highly electronegative carboxyl group. Evidence for the formation of disubstituted pyridine carboxylic acids, and subsequent mechanisms for their formation, compliment the recent identification of these species within carbon-rich chondrites. We can also predict that if interstellar ices contain benzene along with carbon dioxide, benzoic acid ( $\text{C}_6\text{H}_5\text{COOH}$ ) should be formed based on our mechanistical data. This assertion is supported by the discovery of benzoic acid in the Murchison, Tagish Lake [54], and Orgueil meteorites [55].

## Conflicts of interest

No conflicts of interest.

## Acknowledgements

These studies were supported by the US National Science Foundation (AST-1505502) and the W.M. Keck Foundation.

## References

- [1] S. Pizzarello, Y. Huang, M. Fuller, *Geochim. Cosmochim. Acta* 68 (2004) 4963.
- [2] S. Pizzarello, Y. Huang, *Geochim. Cosmochim. Acta* 69 (2005) 599.
- [3] S. Pizzarello, Y. Huang, L. Becker, R.J. Poreda, R.A. Nieman, G. Cooper, M. Williams, *Science* 293 (2001) 2236.
- [4] K.E. Smith, M.P. Callahan, P.A. Gerakines, J.P. Dworkin, C.H. House, *Geochim. Cosmochim. Acta* 136 (2014) 1.
- [5] P. Schmitt-Kopplin, Z. Gabelica, R.D. Gougeon, A. Fekete, B. Kanawati, M. Harir, I. Gebefuegi, G. Eckel, N. Hertkorn, *Proc. Natl. Acad. Sci.* 107 (2010) 2763.
- [6] W. Meinschein, *Nature* 197 (1963) 833.
- [7] M.A. Sephton, *Nat. Prod. Rep.* 19 (2002) 292.
- [8] M.P. Callahan, K.E. Smith, H.J. Cleaves, J. Ruzicka, J.C. Stern, D.P. Glavin, C.H. House, J.P. Dworkin, *Proc. Natl. Acad. Sci.* 108 (2011) 13995.
- [9] G. Cooper, N. Kimmich, W. Belisle, J. Sarinana, K. Brabham, L. Garrel, *Nature* 414 (2001) 879.

- [10] R.I. Kaiser, S. Maity, B.M. Jones, *Angew. Chem. Int. Ed.* 54 (2015) 195.
- [11] S.B. Charnley, P. Ehrenfreund, Y.J. Kuan, *Spectrochim. Acta Part A Mol. Biomol. Spectrosc.* 57 (2001) 685.
- [12] R.I. Kaiser, A.M. Stockton, Y.S. Kim, E.C. Jensen, R.A. Mathies, *Astrophys. J.* 765 (2013) 111.
- [13] K. Kvenvolden, J. Lawless, K. Pering, E. Peterson, J. Flores, C. Ponnampereuma, I. Kaplan, C. Moore, *Nature* 228 (1970) 928.
- [14] N. Raffaelli, *Origins of Life: The Primal Self-Organization*, Springer, 2011. p. 185.
- [15] H.J. Cleaves, S.L. Miller, *J. Mol. Evol.* 52 (2001) 73.
- [16] S.D. Copley, E. Smith, H.J. Morowitz, *Bioorg. Chem.* 35 (2007) 430.
- [17] C.J. Bennett, R.I. Kaiser, *Astrophys. J.* 660 (2007) 1289.
- [18] R.T. Garrod, E. Herbst, *Astron. Astrophys.* 457 (2006) 927.
- [19] R.T. Garrod, S.L.W. Weaver, E. Herbst, *Astrophys. J.* 682 (2008) 283.
- [20] C.J. Bennett, S.-H. Chen, B.-J. Sun, A.H.H. Chang, R.I. Kaiser, *Astrophys. J.* 660 (2007) 1588.
- [21] Y.S. Kim, R.I. Kaiser, *Astrophys. J.* 725 (2010) 1002.
- [22] C.J. Bennett, T. Hama, Y.S. Kim, M. Kawasaki, R.I. Kaiser, *Astrophys. J.* 727 (2011) 27.
- [23] B.J. Sun, C.H. Huang, S.Y. Chen, S.H. Chen, R.I. Kaiser, A.H.H. Chang, *J. Phys. Chem. A* 118 (2014) 7715.
- [24] S.B. Morales, C.J. Bennett, S.D. Le Picard, A. Canosa, I.R. Sims, B. Sun, P. Chen, A. H. Chang, V.V. Kislov, A.M. Mebel, *Astrophys. J.* 742 (2011) 26.
- [25] K.E. Smith, P.A. Gerakines, M.P. Callahan, *Chem. Commun.* 51 (2015) 11787.
- [26] C.J. Bennett, C. Jamieson, A.M. Mebel, R.I. Kaiser, *Phys. Chem. Chem. Phys.* 6 (2004) 735.
- [27] R.I. Kaiser, G. Eich, A. Gabrysch, K. Roessler, *Astrophys. J.* 484 (1997) 487.
- [28] W. Zheng, D. Jewitt, R.I. Kaiser, *Astrophys. J.* 639 (2006) 534.
- [29] O.S. Heavens, *Optical Properties of Thin Solid Films*, Butterworths Scientific Publications, London, 1955.
- [30] L. Zhou, S. Maity, M. Abplanalp, A. Turner, R.I. Kaiser, *Astrophys. J.* 790 (2014) 38.
- [31] G. Baratta, M. Palumbo, *JOSA A* 15 (1998) 3076.
- [32] P.A. Gerakines, W.A. Schutte, J.M. Greenberg, E.F. Van Dishoeck, *Astron. Astrophys.* 296 (1995) 810.
- [33] M. Satorre, M. Domingo, C. Millán, R. Luna, R. Vilaplana, C. Santonja, *Planet. Space Sci.* 56 (2008) 1748.
- [34] C.J. Bennett, C.S. Jamieson, R.I. Kaiser, *Phys. Chem. Chem. Phys.* 12 (2010) 4032.
- [35] K.N. Wong, S.D. Colson, *J. Mol. Spectrosc.* 104 (1984) 129.
- [36] C.J. Bennett, C. Jamieson, R.I. Kaiser, *Astrophys. J. Suppl. Ser.* 182 (2009) 1.
- [37] D. Drouin, A.R. Couture, D. Joly, X. Tastet, V. Aimez, R. Gauvin, *Scanning* 29 (2007) 92.
- [38] Y. Kim, R. Kaiser, *Astrophys. J.* 725 (2010) 1002.
- [39] C.J. Bennett, C.S. Jamieson, Y. Osamura, R.I. Kaiser, *Astrophys. J.* 624 (2005) 1097.
- [40] R.I. Kaiser, P. Maksyutenko, C. Ennis, F. Zhang, X. Gu, S.P. Krishtal, A.M. Mebel, O. Kostko, M. Ahmed, *Faraday Discuss.* 147 (2010) 429.
- [41] C.J. Bennett, R.I. Kaiser, *Astrophys. J.* 661 (2007) 899.
- [42] W.H. Press, B. Flannery, S. Teukolsky, W. Vetterling, *Cambridge University, London*, 1986. p. 521.
- [43] M.E. Jacox, *J. Chem. Phys.* 88 (1988) 4598.
- [44] M. Kumar, R. Yadav, *Spectrochim. Acta Part A Mol. Biomol. Spectrosc.* 79 (2011) 1316.
- [45] L. Wasylina, E. Kucharska, Z. Wegliński, A. Puszko, *Chem. Heterocycl. Compd.* 35 (1999) 186.
- [46] A. Nataraj, V. Balachandran, T. Karthick, M. Karabacak, A. Atac, *J. Mol. Struct.* 1027 (2012) 1.
- [47] R.D. Massaro, E. Blaisten-Barojas, *Comput. Theor. Chem.* 977 (2011) 148.
- [48] M. Karabacak, S. Bilgili, A. Atac, *Spectrochim. Acta Part A Mol. Biomol. Spectrosc.* 135 (2015) 270.
- [49] W. Lewandowski, G. Świdorski, R. Świsłocka, S. Wojtulewski, P. Koczoń, *J. Phys. Org. Chem.* 18 (2005) 918.
- [50] P. Koczoń, J.C. Dobrowolski, W. Lewandowski, A. Mazurek, *J. Mol. Struct.* 655 (2003) 89.
- [51] C.J. Bennett, R.I. Kaiser, *Astrophys. J.* 635 (2005) 1362.
- [52] M. Kumar, M. Srivastava, R.A. Yadav, *Spectrochim. Acta Part A Mol. Biomol. Spectrosc.* 111 (2013) 242.
- [53] Y.-R. Luo, *Handbook of Bond Dissociation Energies in Organic Compounds*, CRC Press, 2002.
- [54] Z. Martins, J. Watson, M. Sephton, O. Botta, P. Ehrenfreund, I. Gilmour, *Meteorit. Planet. Sci.* 41 (2006) 1073.
- [55] Y. Huang, Y. Wang, M.R. Alexandre, T. Lee, C. Rose-Petrucci, M. Fuller, S. Pizzarello, *Geochim. Cosmochim. Acta* 69 (2005) 1073.